Synchrotron-based X-ray micro-tomography: Insights into Sea Ice Microstructure

Sönke Maus[1], Thomas Huthwelker[2], Frieder Enzmann[3], Markus M. Miedaner[3], Marco Stampanoni[2], Federica Marone[2], Manuel A. Hutterli[4], Christoph Hintermüller[2] and Michael Kersten[3]

[1]Geophysical Institute, University of Bergen, email: sonke.maus@gfi.uib.no,[2]Paul Scherrer Institute, Villigen, Switzerland, [3]Institute of Geosciences, University Mainz, Germany, [4]British Antarctic Survey, Cambridge, UK

Abstract

To date most studies of the sea ice microstructure have been based on destructive two-dimensional thin section analysis with little information on pore connectivity, while recent three-dimensional applications of Magnetic Resonance Imaging and X-ray tomography have been resolution-limited to 50-100 microns. During the past decades X-ray micro-tomography based on synchrotron radiation (SXRT) has been accepted as a powerful non-destructive imaging technique in materials sciences. Here we report on first results of three-dimensional, micrometer-resolving imaging of sea ice by means of SXRT. We discuss the strength and limitations of this technique in terms of fundamental scales of the sea ice microstructure and the physical processes associated with them.

1 Introduction

It has long been known that sea ice contains saline brine in pores and fluid inclusions[1,2,3,4,5], while lake ice does only incorporate small amounts of salt in an almost pure ice matrix[6,7]. Sea ice thus differs from freshwater ice in its microscopic structure. The need to focus on the details of the sea ice microstructure has emerged during the past decades in a variety of disciplines. Brine mobility and inclusion sizes strongly influence the mechanical[8,9,10,11,12] and optical[9,13] properties of sea ice, with practical relevance in offshore engineering and remote sensing. They are fundamental to understand the role of sea ice as a habitat of life in polar ecology[14,15,16]. As the microstructure determines the processes of salt entrapment and release, it is also relevant when considering atmosphere-ice-ocean interactions and polar climate[17,18,19,20]. General to all fields is the need to know the distribution of pore networks and inclusions and their influence on macroscopic transport properties, let it be fluid transport, heat and salt diffusion, or the propagation of electromagnetic waves.

Brine entrapment in sea ice is the consequence of its cellular mode of freezing. Under calm conditions sea ice rapidly evolves into a cellular crystal structure of vertically oriented plates, parallel within each grain and with brine layers between them. This lamellar substructure, first described one and a half centuries ago[3,21], is most clearly defined near the ice-water interface[a]. During freezing of natural seawater the lamellar *plate spacing* is 0.2 to 1.5 mm[9,24], while horizontal grain sizes are from a few milli- to centimeters[25,26,9,27,28]. Another known feature are the vertically oriented *brine channels* with diameters 1 to 5 mm[29,30,31,32] and spacings of 1 to 7 cm[33,31,27,34]. In thicker ice 'secondary' *brine channel networks* with larger spacings of 5-20 cm have been described[35,27,36,37]. The conceptual view that has emerged

[a]It is worth a note that Quincke[22,23] gave a first detailed description of the lamellar inclusion-filled structure of saline ice, obtained by freezing solutions of salinities lower than 0.3‰ NaCl. He described the ice as 'foam-like', with many drawings and quantitative observations.

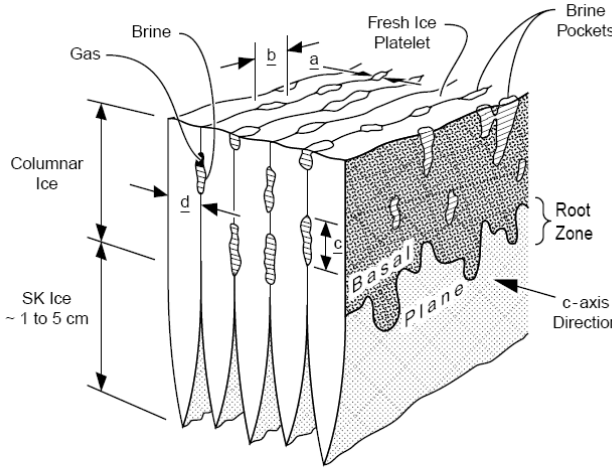

Figure 1: *Three-dimensional sketch of the bottom regime of sea ice, illustrating the separation of brine layers into inclusions, which starts at a distance of* ≈ 1 *to 5 cm from the interface. From ref.*[38].

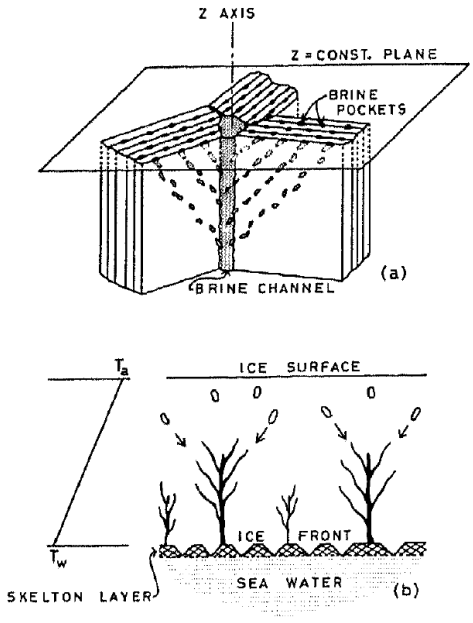

Figure 2: *Upper: drawing of a brine channel fed from the brine layers of surrounding crystals. Lower: Evolution of brine channel networks with distance from the ice-water interface. From ref.*[32].

from laboratory and field investigations is that downward flow through the wider O(1 mm) pores is fed by flow through a finer O(10^{-1}mm) pore network in the original brine layers. Figures 1 and 2 illustrate these principal features of columnar sea ice.

A concise theory of how the microstructure evolves under different growth conditions, essential to formulate fundamental models of the macroscopic physical properties, still needs to be developed. To do so observations of the co-evolution of smallest and largest pore scales during growth and decay are needed. Some fundamental questions in this respect are:

- How do *plate spacing* and crystal size vary with the freezing velocity?
- How are *plate spacing* and crystal orientation related to under-ice currents?
- When does *bridging* between the plates transform the *brine layers* to *pore networks* and what are the preferred length scales and physical mechanisms?
- How do radii and spacing of largest *brine channels* vary with freezing conditions? What is the morphology and permeability of evolving brine channels networks?
- What is the role of hydrodynamics in controling *pore radii* and their *distribution*?
- How do pore scales, shape and connectivity change with *temperature*?
- What are the fractions of *interconnected* and *disconnected pore space*?
- What is the role of *slow diffusion* and *surface energy* minimisation of brine pockets in reshaping pores and their connectivity?

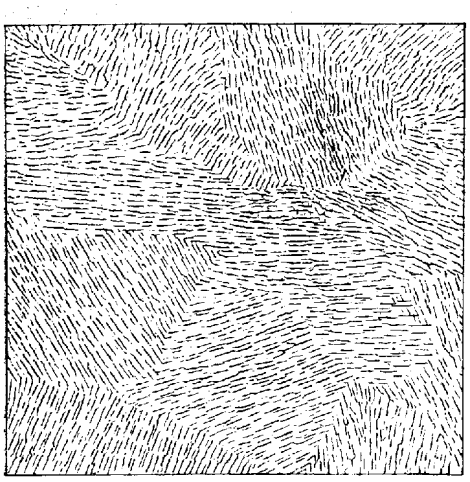

Figure 3: *Tinfoil replica from the bottom of sea ice obtained by E.v. Drygalski[5]. Most individual crystals have a size of* $\approx 2-3$ *cm with parallel ice plates spaced by* 0.5 *to* 1 *mm. Original size* 6×6 *cm.*

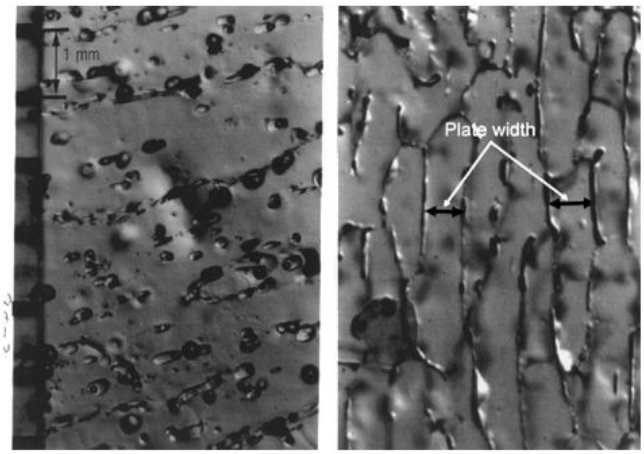

Figure 4: *Horizontal thin section micrographs of first-year ice from ref.[12]. Right: obtained in situ within several hours after sampling. Left: stored below the eutectic temperature* -23 *°C for several months, then warmed to* -10 *°C prior to imaging. Images are* $\approx 5 \times 7$ *mm.*

In the following a short account of the present knowledge of these topics on the basis of microstructural observations techniques utilised to date will be given. Then the potential to make progress on the basis of synchrotron-based X-ray microtomography (SXRT), a technique that we have recently tested on laboratory grown sea ice samples, is discussed.

2 Imaging techniques of sea ice microstructure

The microstructure and salinity of sea ice have already received some interest during the first polar expeditions. Scoresby[1] described that sea ice contains salt in form of liquid brine in the interstices of ice crystals, while Walker[3] pointed out a 'vertically striated structure' that was most apparent near the ice-water interface. The first documented image of this lamellar crystal substructure of natural sea ice is probably a tin-foil replica obtained by E. v. Drygalski more than 100 years ago (Figure 3). First photographs of vertical and horizontal sea ice sections, illustrating larger pores and brine channels, were documented by Hamberg[4], who also pointed out another important aspect of sea ice in contrast to lake ice: While the orientation in the upper centimeters of sea ice is often random, crystals with vertical c-axis are eliminated rapidly during further growth[b], and no exceptions to this rule were found since then[9].

Our present knowledge of the sea ice microstructure is still mainly based on the analysis of two-dimensional thin sections similar to Figure 3 from Drygalski. It is therefore useful to first recall the main procedure and shortcomings of this technique.

[b]For primary sea ice, which contains considerable amounts of brine between the basal plane plates, the anisotropic effective conductivity, parallel heat conduction in a laminate of different conductivities exceeding serial heat conduction, is the most likely mechanism of geometric selection[39,40]. For lake ice the selection mechanism of crystal orientation is still a matter of debate[41,42,43,6,44].

Two-dimensional thin section analysis

Columnar sea ice, to be considered here as the dominant Arctic ice type, is structurally highly anisotropic, and the preparation of horizontal thin sections, similar to Figure 3, is most effective in extracting geometrical information. The standard approach of thin section analysis begins with cutting slices from a vertical ice core, which are then reduced in thickness with help of a microtome[45,9,46,47,48]. If thin enough slices are prepared this approach allows to obtain micrographs wherein brine inclusions of 0.01 mm or even smaller in size are distinguishable[45,49]. As an example Figure 4 from ref.[12] shows the fine structure of brine inclusions within a single crystal. However, analysing and interpreting such images has been limited by two aspects. In the most extensive statistical descriptions to date the digitized pixel size was 0.03 mm, limiting the resolvable inclusions to approximately two times this scale[50,46]. Such a resolution limit is no longer a problem with present day computing and image processing capabilities. However, with regard to future application of thin section analysis, another problem remains and adds to the lack in three-dimensional information. The sample preparation process is elaborative and susceptible to a reaction of brine inclusions to the procedure[51]. To date it has not been studied to what degree the destructive sectioning process effects the details of the inclusion structure.

Sampling and storage

A general problem of all imaging techniques, which adds to the destructive sectioning process of thin sections, is related to sampling and storage. Sea ice is a reactive medium which rapidly changes its morphology when removed from 'in situ' conditions. This makes the interpretation of micro-structural observations often problematic. A frequently applied procedure is 1. sampling, 2. cooling, 3. storage, 4. warming, 5. analysis[46,49]. This implies (i) thermal hysteresis due to the freezing and remelting of pores and (ii) metamorphosis by slow diffusion processes during storage. Although the relative role of these processes has not been investigated yet, it has become clear that their joint effect fundamentally changes the pore structure, even after storage below the eutectic temperature. An example is shown in Figure 4 from ref.[12], comparing a thin section image obtained *in situ* within several hours after sampling with one of the same ice after several months of storage below the eutectic temperature -23℃. Being an extreme example, because cooling below the eutectic point is expected to change the inclusion structure by salt precipitation, it indicates the difficulties to obtain information about the *in situ* microstructure from stored and thermally modified samples. The problem may be overcome to some degree by rapid analysis in the field, shortly after sampling[47,12], or by centrifugation of a sample before storage, removing the brine and making the sample less reactive[52,48]. As discussed below, the latter method is of interest in connection with synchrotron-based X-ray microtomography.

Three-dimensional imaging techniques

Besides its destructive nature, another drawback of thin sectioning is its lack in three-dimensional information. Early applications of three-dimensional non-destructive imaging have utilised two techniques, X-ray computed microtomography (XRT)[53] and Nuclear magnetic resonance imaging (NMR)[54], yet were resolution-limited to millimeter-sized pores. An order of magnitude better resolution has been recently obtained with NMR to provide statistics of brine inclusions on the basis of 0.09 mm pixel size[48]. The latter is still a clear

limitation at low temperatures, when inclusion sizes are small. For example, in ref.[48] a 50 % difference in imaging and phase-relation derived brine porosities was found at low temperatures, and interpreted in terms of this resolution limit. A similar conclusion was drawn in ref.[46] due to an increasing number of inclusions during warming. In a later NMR study[55] even larger discrepancies were found, with under- and overestimates of brine volumes for columnar and fine-grained granular ice, respectively. Serial thin-sectioning has been used to validate NMR imaging results[48], indicating reasonable agreement of average pore size and porosity when the latter is relatively high (≈ 0.2). However, much higher pore size standard variations, for thin section images compared to NMR, indicate the loss of details by this method and pixel sizes limited to 0.09 mm.

XRT with increased resolution (voxel size $20-40$ μm) has been applied to derive porosity and pore sizes of polar firn[56] and snow[57,58], where the most important scales are of millimeter size and clearly above this resolution limit. Recently, XRT imaging of ice grown from NaCl solutions in the laboratory has been reported[59]. In the latter study the voxel size of 40μm was a slight improvement on most earlier two- and three-dimensional studies with resolutions $\approx$ 50 to 100 μm[46,47,48]. As shown by a recent high resolution optical study[49] and our preliminary observations this is still insufficient to characterise pores and pattern evolving from original brine layers. Many air-filled pores in Figure 5, corresponding to centrifuged brine, have diameters less than 50 μm. Thus, a voxel size of 5 to 10 μm appears necessary to resolve them and properly image pore networks in sea ice. For salt crystal identification even a voxel size of 1 micron seems necessary[49].

Synchrotron-based X-ray tomography

During the past decades, tomography based on highly brilliant and coherent X-ray synchrotron radiation has been accepted as a powerful imaging technique in materials sciences[60,61]. Very recently, synchrotron-based X-ray micro-tomography (SXRT) was used to image hailstones and partially frozen multiphase systems with similar salt content as natural sea ice[62,63]. The technique allows three-dimensional imaging of centimeter-sized samples with micrometer resolution. While portable XRT scanners are often operated in a cold room[56], in the latter studies a special setup has been developed to cool the samples during imaging and keep them at 240 K or lower temperatures[62,63]. We have recently applied SXRT with this setup to obtain, for the first time, three-dimensional images of laboratory-grown seawater ice at the TOMCAT-beamline of the Swiss Light Source[c]. Results of this study will be presented elsewhere[?] . Here we shall, on the basis of a few images, discuss the potential of this method to characterise essential features and evolution processes of the microstructure of sea ice.

SXRT is based on absorption and allows, for sea ice, a clear discrimination of air, ice, and solid salts. We have used two sampling/storage protocols that take advantage of these absorbtion contrasts. The first applied procedure was (i) rapid centrifugation of a sample at the local *in situ* temperature, (ii) storage and transport in a low temperature freezer or dewar and (iii) imaging at subeutectic temperature.[d]. The strength of this approach is

[c]The present capabilities at the TOMCAT-beamline of Swiss Light Source (SLS, Paul Scherrer Institute, Villigen, Switzerland) allow field-of views ranging from 0.75×0.75 to 11.45×11.45 mm^2 with a theoretical resolution of 0.35μm and 5.6μm, respectively.

[d]The imaged samples had $\approx 1 - 1.5$ cm diameter and height, and were prepared manually on dry ice from centrifuged larger slices of both 3 cm thickness and diameter.

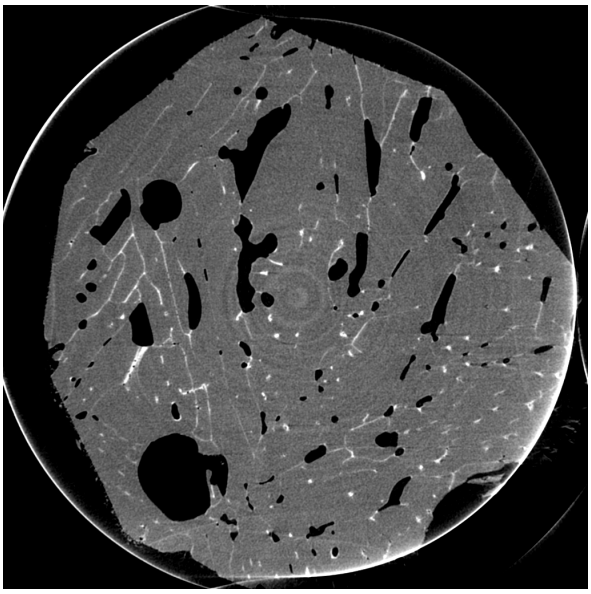

Figure 5: *Horizontal slice of a centrifuged laboratory-grown sea ice sample obtained by by SXRT at* $\approx -30℃$*. The image is* ≈ 12 *mm on a side, obtained with a voxel size of 5.6* μm *binned two times. Air (pores emptied by centrifugation) appears as dark, ice as grey and salt crystals (corresponding to entrapped brine) as white. Note that the whole sample comprises 300 slices all spaced in the vertical by 5.6* $\times 2$ μm*.*

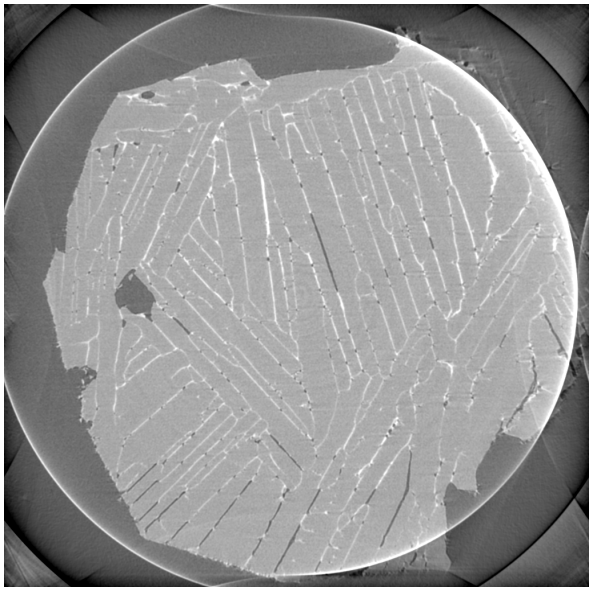

Figure 6: *Horizontal slice of laboratory-grown sea ice, rapidly cooled below* $\approx -50℃$ *after sampling, obtained by SXRT at* $\approx -30℃$*. The image is* ≈ 12 *mm on a side, with 5.6* μm *voxel size binned two times. Ice appears as grey, air as dark, salt crystals as white. As the image was not centrifuged most air indicates 'lost brine'. Also here the vertical spacing of slices is 5.6* $\times 2$ μm*.*

that it yields information about the pore connectivity that ice has in situ, and allows to distinguish between the connected and disconnected pores. Figure 5 shows a horizontal slice of an SXRT image obtained with original voxel size 5.6 μm, binned two times. The centrifuged pores appear dark (as air), the trapped inclusions (salt) as light, and the ice as grey. The vertical distance of slices as in figure 5 is also 5.6 $\times 2$ μm, sufficient to resolve the network connectivity of the finest pores (see Figure 9 below).[e] The sample in Figure 5 stems $\approx$ 3 cm from the surface of 11 cm thick ice and several wide brine channels have already formed. The method and resolution preserves the main network characteristics relevant for evaluation of its transport properties. In the second sampling protocol the sample was not centrifuged, but a 3 cm thick slice from an ice core of 10 cm diameter was immediately put into a -80 ℃ freezer. The sample shown in Figure 6 thus does not resemble the true pore morphology of sea ice. It does, however, well illustrate the lamellar crystal substructure and distribution of plate spacings. The brine layers contain air bubbles that are likely related to contraction upon transition of brine to solid salts. Some larger air pores are eventually related to loss of brine during sampling, as the shown sample comes from a high mobility level, $\approx$ 3 cm near the ice-water interface. The $\approx$ 1 mm wide air pore, visible at a crystal junction near the left edge of the image, is very probably attributable to such brine loss.

[e] In the present setup images were limited to $\approx$ 4 mm vertically, yet longer samples can be imaged by stacking.

3 Pore scales and related physical processes

The evolution of microstructural pattern in growing sea ice may be roughly classified into three principal regimes. The first regime (I) comprises morphological instabilities that evolve due to an interplay of heat and solute diffusion, the most prominent pattern being the plate spacing to which a cellular freezing interface adjusts. Here the primary lamellar skeleton of young sea ice is determined. The second regime (II), proceeding upward from the freezing interface toward lower temperatures, is characterised by a strong decrease in the brine porosity. This decrease is not only controlled by cooling and fractional freezing but also by desalination due to convective motion. The latter is associated with the formation of channelised fluid paths found in many materials and environments[64,65,66]. This transition from a laminate to a network of pores is a particular important aspect for the sea ice medium. The third regime (III) is reached when desalination becomes small and porosity changes are due to cooling and diffusion only. Some important questions in regime (III) are how inclusion shapes change during freezing, if and how pore networks disconnect, what happens during pressure buildup in disconnected pores, and to what degree slow surface energy minimisation may take place. In the following the potential role of SXRT to improve our understanding of these regimes is discussed by considering them in increasing order.

Plate spacing, crystal size and orientation

Recent work indicates that the plate spacing of sea ice can be reasonably predicted by a macroscopic variant of the Mullins-Sekerka[67] morphological stability theory[68,24,69]. The approach has been mainly validated by plate spacing observations based on thin section analysis, and at first glance it does not appear necessary to apply SXRT to obtain this O(1 mm) structural scale. However, Figure 6, obtained from a sample close to the freezing interface, shows many details of these pattern at junctions and crystal boundaries. These can be of interest in the study of the plate spacings dependence on growth conditions. The increase in plate spacing with decreasing growth velocity must, for example, be accompanied by overgrowth of plates, while accelerated growth would lead to splitting. Figure 6 indicates that SXRT will be useful to study the details of these transitions. A related problem is the frequently observed crystal c-axis alignment with ocean currents[70,71,72,73]. Three-dimensional near-bottom microstructure resolution by SXRT can essentially improve our understanding of the morphological adjustment to periodic changes in the under-ice flow[74,75] and the response to extreme currents, e. g., ref.[48].

Plate spacing observations in older ice may, *vice versa*, provide indirect information about its growth velocity[76,24]. However, due to the mentioned morphological transition to networks, plate spacings are in general less clearly defined in aged ice and far from the freezing interface, e.g., ref.[76,46] or Figure 4 above, where the plate spacing may only be identified by trains of pores. A comparison of plate spacings measured by thin section analysis rapidly in the field with measurements after storage[77] shows that metamorphosis of brine layers makes such observations uncertain. Here SXRT of samples stored at low temperatures can be a useful technique to improve the accuracy. The required resolution can be estimated by considering a 100 μm brine layer of salinity 50-100 ‰ that is cooled below its eutectic point. Conversion to solid salt will shrink it by a factor of ten to twenty. Figure 5 was obtained with a voxel size of 5.6 μm, binned two times, thus being at the upper limit to capture these features. As seen in Figure 5, a horizontal image $\approx$ 8 cm from the

bottom of 11 cm thick ice, the salt crystal signal in the original brine layers becomes weak, but plate spacings can still be identified.

To quantify grain sizes which generally are of order O(1 cm) in sea ice[26,25,27,28] SXRT is of course not useful. However, the morphology at grain boundaries and junctions can be studied in some detail. The field of view in our setup has been sufficient to include a few of these features in a typical SXRT image. By resolving the lamellar plate spacing pattern, also crystal orientations are easily identified from the tomographic images.

Transition of brine layers

The transition of brine layers near the bottom of sea ice has been described qualitatively as a two-stage process[78]. A transition to sheet-like pattern starts at a distance of 2 to 4 cm from the ice-water interface, while a subsequent separation into elongated pores appears to take place at a $\approx$ 10 cm distance. While the former scale is consistent with observations of the low-strength skeletal layer[68,69], quantitative observations of the second morphological change within the brine layers are almost completely lacking. Some observations of 'pinch-off' of brine pockets indicate its onset when brine layers have to shrink to a width of $\approx 0.05 - 0.1$ mm[79,31]. A value of 0.07 mm has been noted as the 'minimum layer width before splitting of brine layers'[80] and may eventually be interpreted as a lower bound. However, direct observations and detailed statistics of pore changes near the interface are not available yet, and here high-resolution SXRT has a large potential.

A concise theoretical explanation for the bridging is still outstanding. The minimisation of surface energy, as frequently suggested[81,80,82,83], is unlikely to be relevant in the bottom regime of strong cooling and convective transport of heat and solute. It may also principally be rejected because the brine layers are minimum energy surfaces[68]. An theoretical study of the droplet 'pinch-off' from a pore[84] indicates that the problem is similar to Rayleigh's instability of an inviscid liquid jet[85], the formal difference being that the transport in the pore is not dynamical yet diffusive. For alloys the predicted pinch-off wave length of $\pi/0.697 = 4.508$ times the diameter agreed reasonably with experiments[86] and numerical simulations[87]. The pinch-off was found to be triggered by fluctuations in the growth velocity. This behaviour is qualitatively similar to what Harrison[79] has described as 'solute transpiration pores' in ice, which started to break up into droplets when the motion of the temperature gradient was halted, creating thermodynamic disequilibrium. For growing sea ice these ideas likely need to be modified and extended due to the presence of convection. A plausible mechanism is that density fingering in the brine layers leads, in connection with upward flow of less saline seawater, to pattern of supercooling with preferred freezing[68]. Once the resistance is locally increased by thinning, the flow will slow down and subsequent lateral freezing enhances the heterogeneity, finally leading to bridging and a pore network.

Lacking a concise theoretical concept the width of brine layers at the onset of bridging has been estimated in two ways[68]. First, thin section pore size statistics of ice samples not two far from the interface[46,47] have been extrapolated to porosities typical at the top of the skeletal layer. To do so a relation between inclusion sizes and brine porosity based on warming of the prepared thin sections, see below, has been applied. A second estimate has been based on interpretation of a change in the strength-porosity relationship at the top of the lamellar bottom skeletal layer[68]. Both estimates are indirect and crude, yet indicate a most plausible value of $0.08 < d_{sk} < 0.12$ mm for the width d_{sk} of brine layers at the onset of bridging.

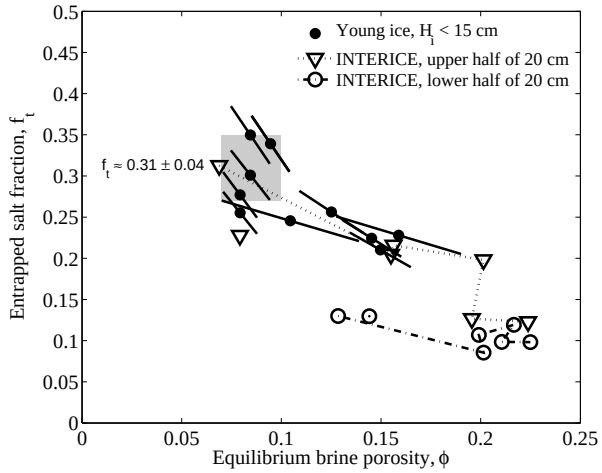

Figure 7: *Fraction of salinity that could not be removed by centrifugation at in situ temperatures, interpreted as the disconnected pore fraction f_t. Solid circles: thin ice grown from seawater in the laboratory. The errorbars indicate the uncertainty in the porosity due to bulk ice temperature and salinity observations. Triangles: Warming sequence of upper half of 20 cm thick ice grown in a large tank[89]. Note the lower disconnected pore fractions in the lower half (open circles), consistent with an incomplete metamorphosis of brine layers. During warming the fraction f_t stays rather constant (upper half), until a value of $\phi \approx 0.2$ is reached. Porosities are based on bulk salinity and temperature assuming thermodynamic equilibrium.*

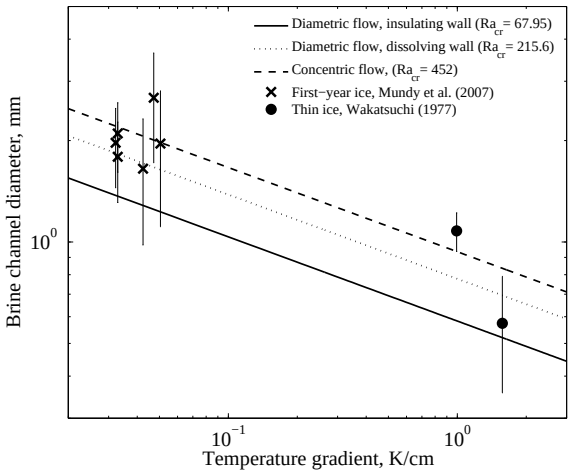

Figure 8: *Quasi in situ determinations of brine channel diameters at the bottom of sea ice. Crosses: photographic under-ice observations from ref.[90], temperature gradients being based on the observed average ice thickness and reported ice surface temperatures, assuming a linear temperature gradient and the ice bottom at the freezing point of ≈ -1.8℃. Circles: optical observations of the widths of streamers emerging from the bottom of rapidly growing thin laboratory seawater ice[33]. The temperature gradient in the latter high salinity young ice was reduced by 0.8 with respect to freshwater ice growing at the same velocity, consistent with parallel observations[91] and theoretical expectations[68]. The lines are theoretical critical Rayleigh numbers for convective onset, e.g.,[92].*

The accurate determination of the bridging transition is important to solve the salt entrapment problem in sea ice in general, with implications for the vertical extent of the high-mobility and low-strength skeletal layer and relevance for problems of sea ice geophysics and ecology. A simplistic model that treats bridging as a two-dimensional percolation process appears to perform well in predicting salt entrapment[68,69]. To date only a few images of the morphology of bridging have been obtained by thin-sectioning in the plane of former brine layers[47,12,88]. Being rather tedious, this approach likely involves destruction of brine layers and bias by phase changes. Non-destructive SXRT of centrifuged samples from the bottom regime of sea ice may be very effective to resolve the bridging pattern of brine layers with micrometer resolution, to be interpreted in terms of the hydro- and thermodynamics that drive their formation.

Disconnected pore fraction

The bridging process implies the formation of disconnected pores within the brine layers. If several samples of the same ice are available this fraction f_t may be computed from $f_t = S_c/S_i \times (S_i - S_c)/(S_b - S_i)$, where S_i is the bulk salinity of the original ice sample, S_c the residual of a second sample after centrifugation at in situ temperature, and S_b the salinity of the brine obtained by centrifugation. The underlying assumption is that the brine salinities in the connected and disconnected pore space are the same. Alternatively S_i can be computed from the mass and salinity of the centrifuged brine and ice samples[52]. In Figure 7 the disconnected salt fractions of growing young ice are compared to estimates based on salinity observations of warming young ice grown under similar conditions[89]. At lowest porosities the entrapped pore fraction appears to saturate at a value of $0.3 < f_t < 0.4$, an upper bound supported by field observations[52,93]. However, the results in Figure 7 do not extend to low porosities, and the present values of ϕ are indirect calculations based on thermodynamic equilibrium. As the latter tends to overestimate the brine salinity and underestimate the porosity[94,95], the data in Figure 7 need to be interpreted with caution. The true porosities for the young ice in Figure 7 (solid circles) are not below $\phi \approx 0.1$[93]. It is noted that a considerably smaller 'fractional connectivity', comparable to the present $(1 - f_t)$, has been recently reported for laboratory grown NaCl-ice on the basis of XRT imaging[59]. The latter authors report a connectivity that decreases sharply below $\phi \approx 0.1$ and ceases near $\phi \approx 0.03$. However, their results are based on unidirectional connectivity within 1 cm samples, determined by warming a cut sample (not *in situ*), and limited by 40 μm voxel size.

An interesting aspect in Figure 7 is that f_t appears to stay rather constant during warming sequences. Such a saturation value is comparable to the ratio of salinities of thick multy-year to first-year ice, indicating that the fraction of entrapped pores is controlled by the early evolution and bridging process (open triangles and circles). The knowledge of the entrapped pore morphology is also important to understand ion fractionation and its evident dependence on ice type, growth conditions and temperature history[96,97,98,99]. The many pores with diameters of 50 μm in Figure 5 thus indicate that a proper imaging of the process of solute entrapment requires imaging with micrometer resolution. SXRT distinction of air, ice and solid salt in centrifuged samples is a promising technique for doing so properly, while recent XRT work[59] is likely resolution-limited.

Brine channels

In early studies wide 'brine channels', with 1-5 mm diameters, were tentatively associated with the desalination of *warming* sea ice[4,100]. Their existence in *cooling* sea ice during the growth phase was first described in ref.[35,101]. Lake and Lewis[29] then outlined, mainly on the basis of temperature fluctuations, the basic mechanism of salt release from sea ice: downward convective motion of brine-rich streamers is balanced by upward moving waters around them. Experiments in thin growth cells have confirmed this view[30,31] and raised the interest in their quantitative description. For very thin ice maximum channel diameters of $1-3$ mm have been found[30,31,27,48], with a $1-7$ cm spacing of major channels that decreased with freezing rate[33,31,102,32,27,37,103]. In 1 to 2 m thick ice, by the end of the growth season, a category of wider $5-10$ mm channels spaced by $\approx 10-20$ cm has been reported[35,29,104]. These widest pores only account for a small fraction of the overall porosity, compared to their radial feeders of 2-3 cm extension[27,29] and diameters in the range $2-8$ mm[29].

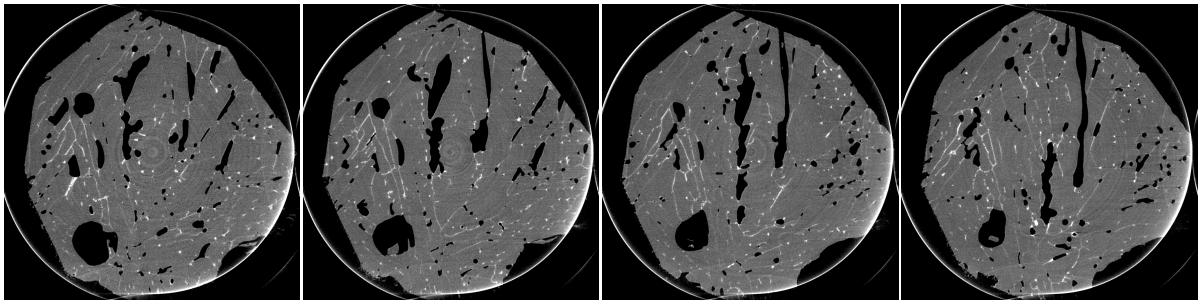

Figure 9: *Horizontal images of a centrifuged young ice sample obtained by SXRT at* $\approx -30\,℃$*. Voxel size is* 2×5.6 μm*, images are* ≈ 12 *mm on a side, and spaced vertically by* 220 μm*. Air (pores emptied by centrifugation) appears as dark, ice as grey and salt crystals (corresponding to entrapped brine) as white.*

What limits the width of the largest pores? Lake and Lewis[29] considered a hydrodynamic stability bound, evaluating the condition for the onset of convection in a vertical tube

$$\frac{D_{cr}}{2} \geq \left(\frac{Ra_{cr} \kappa_s \mu}{g d\rho/dz} \right)^{1/4}, \tag{1}$$

where μ and κ_s are dynamic viscosity and solute diffusivity of the brine. The density gradient $d\rho/dz$ is computed under the assumption, also here, that the density-controlling brine salinity is in thermodynamic equilibrium with temperature. The minimum diameter D_{cr} for convective onset is then given by the critical Rayleigh number $Ra_{cr} = 67.95$, corresponding to the most dangerous mode of diametric flow in an infinite cylinder with insulating boundaries, e.g.[92]. It depends slightly on temperature, yet is mainly controlled by the temperature gradient. At -3 ℃ and dT/dz between 0.05 to 1 K/cm, the range of growth conditions of most natural sea ice, one expects diameters of $1.2 > D > 0.6$ mm for the onset of convection. In Figure 8 under-ice observations of channel widths and outflowing streamers are compared for two studies[33,90], indicating that the channels operate at larger Rayleigh Numbers. Observations appear more consistent with either a conducting boundary condition for diametric flow (corresponding to a dissolving wall), or with a coaxial flow mode (boundary conditions not being relevant), for which Ra_{cr} takes larger values of 215.6 and 452, respectively[92]. On the one hand, Figure 8 appears to be a promising predictor for the width of brine channels by marginal convective stability. On the other hand, it is unclear why it should not occur at the most dangerous mode of diametric flow.

Taking into account the observed channel width aspect ratios of 1.3 to 1.5[90] may only explain part of the apparent discrepancy[92]. However, the standard deviation in the latter study apparently can do so, which would be consistent with channel throats controlling the convection. Looking at the complex shape of the widest pores in Figure 5, and their vertical variability on length scales of a millimeter indicated in Figure 9, shows a complex structure. To validate if, and in which mode brine channels operate at marginal hydrodynamic stability, their morphology needs to be resolved properly. For the longterm evolution of brine channels, and aspects like the onset of desalination in the spring season, the connectivity to the ambient fine-scale pore network is likely to play a role, again requiring micrometer resolution. The above mentioned reports of rather wide channels with diameters of 5-10 mm were

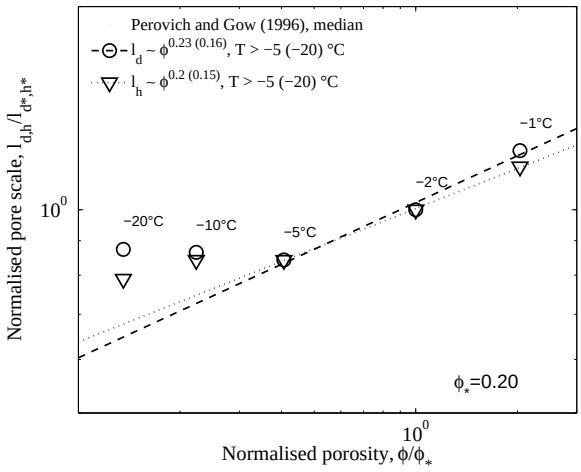

Figure 10: *Normalized minor (l_d) and major (l_h) axis length of pores in a horizontal thin section warmed in the laboratory*[46]*. l_d was computed by dividing the median cross-sectional area by the major axis. The data are normalised by the values at $-2℃$, and power law fits are given for the warmer $> -5℃$ subset and the whole temperature range (in brackets). Porosities are based on thermodynamic equilibrium.*

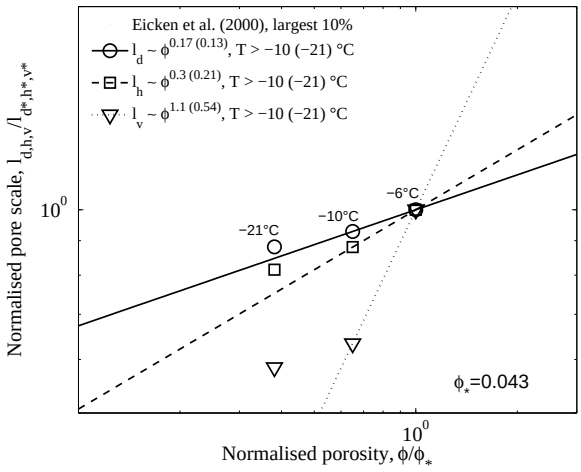

Figure 11: *Normalized minor (l_d) and major (l_h) axis length in a horizontal, and major axis length (l_v) in a Nuclear Magnetic Resonance image slice (thickness 0.4 mm), warmed in the laboratory*[48]*. The data are normalised by the values at $-6℃$, and power law fits are given for the warmer subset and the whole temperature range (in brackets). Porosities are based on thermodynamic equilibrium.*

based on relatively crude optical observations of two-dimensional cross-sections, while more detailed thin section analysis indicate that pore diameters larger than 5 mm are seldom observed[102,31,105,37,48,90]. The detailed morphology of wider channels also remains unclear.

Temperature dependence

The basic effect of cooling or warming sea ice is to change its brine porosity by additional freezing or melting until the interstitial brine reaches thermodynamic equilibrium. However, porosity changes are, as mentioned above, not only associated with local temperature changes. Upward movement of less saline brine does, after rapid thermal equilibration, also imply freezing. The relation between porosity and temperature will thus be different for bottom regimes influenced by convection and for ice levels where fluid movement has almost ceased. As localised convection may create larger thermodynamic disequilibrium than uniform unidirectional freezing, it may be susceptible to thermodynamic instabilities and create different length scales. In other words: The shape of a pore may change in a different way than during slow equilibrium freezing and its change may be irreversible. Another hysteresis effect is inherently given by the expansion of brine upon freezing, leading to expulsion of fluid. During warming this process can neither be reversed, as the seawater at the interface is in most cases less saline than the effectively expelled brine.

These complications in the temperature-porosity relationship in real sea ice make interpretations of cooling-warming scenarios of laboratory samples, susceptible to metamorphosis during storage, even more difficult. In contrast to redistribution in the field[68], expelled brine is always lost from laboratory samples[106]. Moreover may the mode of cooling/warming be

different from field conditions, and the irreversible convection through the boundaries may have other consequences for the internal redistribution of brine and the change in pore shapes and connectivity. In general are these processes, and thermal hysteresis during transport and storage, a serious problem in the preparation process of samples from naturally grown sea ice, recall Figure 4. As an example, a recent high-resolution optical study of the temperature-dependence of pore shapes and sizes[49] is mentioned. The authors analysed first-year ice from a field program for which the microstructure was also investigated on broader scales and growth conditions well reported[28,47]. The investigated samples came from the depth levels 60 to 80 cm in 1.7 m thick ice, and were obtained by the end of the winter at an in situ temperature of ≈ -5 ℃. At that time the ice was already in a stage of warming, originally having been cooled to ≈ -12 ℃ in mid-winter at the levels in question. Micrographs of this ice were taken at a temperature of -15 ℃, but only after storage at -20 ℃ for 3 years. Hence, in addition to the thermal cycling, slow diffusion and surface-energy minimisation mechanisms can be expected to have been active, and it is uncertain to what degree the results longer reflect the microstructure of sea ice *in situ*.

These limitations should be kept in mind when considering the few studies of the temperature dependence of pore dimensions, all based on imperfect storage procedures and warming of samples in the laboratory[50,46,48,55]. Some principal results of two studies[46,48] are summarised in Figures 10 and 11. To do so the reported porosity-dependence of inclusion lengths scales has been evaluated in the form

$$l_d \sim \phi^{e_d}, \qquad l_h \sim \phi^{e_h}, \qquad l_v \sim \phi^{e_v}, \tag{2}$$

where l_d and l_h are the minor and major axis lengths in a horizontal cross section (corresponding often to the directions normal and parallel to the original brine layers) and l_v the vertical axis length. A similar exponent e_n may be used to describe the number n of pores. If inclusions do not split or merge and n is constant, the constraint $e_d + e_h + e_v = 1$ is expected. One has, for example $(e_d = 1, e_h = e_v = 0)$ for a laterally shrinking vertical brine layer, and $(e_d = e_h = 1/2, e_v = 0)$ for a vertical circular cylinder that changes only its diameter. For the two studies the resolution and typical horizontal length scales were 0.03 and $0.05 - 0.3$ mm in ref.[46], Figure 10, while they were 0.09 and $0.2 - 1$ mm in ref.[48], Figure 11. Also porosities were very different. Exponents e_d and e_h were however similar, at higher temperatures in the range $0.17 - 0.30$. The dependence is weaker when including data at lower temperatures included (given in brackets in the figures), which in both studies has been associated with the resolution limits, leaving the smallest pores undetected. The vertical pore length, investigated in ref.[48], shows a much stronger porosity-dependence. If also the observed number exponents for vertical pores ($e_n = -0.13(-0.27)$, not shown) are considered, one obtains $e_d + e_h + e_v + e_n \approx 1.44(0.61)$[f]. This indicates not only undetected pores at low temperatures ($0.61 < 1$), but also a discrepancy at higher temperatures ($1.44 > 1$). A likely explanation is that vertical thin sectioning of sea ice (and the finite NMR slice thickness of 0.4 mm in the study) does not retrieve the vertical pore lengths, but rather the inclination of the pores. This again points to the need of three-dimensional observations, in addition to the necessary increase in resolution.

Conclusions and quantitative results from an earlier study of horizontal sections[50] are similar. To evaluate how realistic porosity changes in natural sea ice may be resembled by

[f]The value in brackets includes also observations at lowest temperatures, when resolution limits were reached

warming/cooling of laboratory samples requires more statistical descriptions of that kind. While direct observations of three-dimensional pore connectivity changes with temperature may, at highly improved resolution, be obtained by SXRT on centrifuged field samples, the intrinsic behaviour of disconnected inclusions shapes is more difficult to find out. During storage in the liquid phase these will likely approach shapes that relate to the high anisotropy of the ice-water interfacial energy[107,108], whereas in the field, under a temperature gradient and permanent thermal cycling, they may not do so. Here sophisticated sampling, storage and imaging procedures could become necessary. An empirical description of the shrinking, merging and splitting behaviour of pores in a form like equation (2) would be useful for proper optical modelling of sea ice[109] and could be used for conceptual parameterisations of its transport properties by network models[105,110,111].

It is further important to develop a better understanding of the physical processes that lead to merging and splitting itself. In addition to pore shapes, hysteresis has also been observed for the phase transition process, very small inclusions apparently becoming supercooled until they change phase spontaneously[112,113]. The formation mechanism of smallest inclusions reported in sea ice[47,49] and pressure-related figures due to the expansion of trapped brine pockets[114,35,78,88] is presently not understood. It might be more probable during rapid cooling of a sampled core than it is under slowly changing natural conditions. However, the occurence in bands near the bottom[35,88] indicates a formation that relates to hydrodynamic interactions with the seawater. A related question is when pores split into spheres. In some figures of ref.[49] strings of very small inclusions with sizes ≈ 0.02 to 0.03 mm are seen, while below a length scale of 0.03 to 0.04 mm the inclusion aspect ratio in their sample approaches unity. Similar scales appear in a study of artificial pores[79]. That micrographs from ref.[49] during a cooling sequence do not manifest a splitting behaviour of the thinnest (≈ 0.03 to 0.04 mm) elongated inclusions, also indicates the role of surface energy as a driving source. Micrometer-resolving SXRT can shed new light on the latter problems.

4 Summary

Sea ice is a reactive porous medium with a pore structure that is to first order lamellar near the freezing interface, but becomes increasingly complex during further cooling, with distance from the interface. This happens by an interaction of hydrodynamic and thermodynamic instabilities with vertically directed diffusive and convective exchange of heat and salt with seawater, on which sea ice floats. Due to a change in temperature gradients, boundary conditions and thermal hysteresis upon freezing/melting it is not easy to find sampling and storage procedures that preserve its microstructure characteristics. One always has to find a trade-off between resolution, effort and the physical process one wants to observe. We have summarised the most relevant length-scales and mechanisms during the microstructure evolution like (i) plate spacing selection and crystal orientation, (ii) bridging of plates and pore network formation, (iii) fractionation of connected and disconnected pore space, (iv) brine channel morphology and convective stability and (v) temperature and porosity-dependence of pore scales, and argued for the need of three-dimensional observations with micrometer resolution, not available to date. Preliminary results of imaging laboratory-grown samples by synchrotron-based X-ray microtomography (SXRT) indicate that, in connection with proper sampling and storage, SXRT has a large potential to make such observations, and advance models of the sea ice microstructure and its macroscopic behaviour.

References

[1] W. Scoresby, *Mem. Wernerian Society*, 1815, **2**, 328.
[2] G. F. Parrot, *Ann. d. Physik*, 1818, **57**, 144.
[3] D. Walker, *Proc. Royal Soc. London*, 1859, **9**, 609.
[4] A. Hamberg, *Svenska Vetenskapsakadamien, Bihang til Handlinger*, 1895, **21**, 1.
[5] E. Drygalski, *Grönlands* E*is und sein* V*orland*, vol. 1 of *Grönland-Expedition der Gesellschaft für Erdkunde zu Berlin 1891-1893*, Berlin, Kühl, 1897, 555 pp.
[6] P. Hobbs, *Ice Physics*, Clarendon Press, Oxford, 1974, 837 pp.
[7] V. F. Petrenko and R. W. Whitworth, *Physics of Ice*, Oxford University Press, 1999, 373 pp.
[8] B. Michel, *Ice Mechanics*, Les Presses De L'Université Laval, Québec, 1978, 499 pp.
[9] W. F. Weeks and S. F. Ackley, in *The Geophysics of Sea Ice*, vol. 146 of *NATO ASI Series*, Plenum Press, pp. 9–164, ed. by N. Untersteiner.
[10] T. J. O. Sanderson, *Ice Mechanics - Risks to Offshore Structures*, Graham & Trotman, 1988, 253 pp.
[11] E. M. Schulson, *Eng. fracture mech.*, 2001, **68**, 1839.
[12] D. M. Cole, *Eng. fracture mech.*, 2001, **68**, 1797.
[13] F. D. Carsey, *Microwave Remote Sensing of Sea Ice*, vol. 68 of *Geophysical Monograph*, American Geophysical Union, Washington, 1992.
[14] R. A. Horner, *Sea ice biota*, CRC Press, 1985.
[15] I. A. Melnikov, *The* A*rctic* S*ea* I*ce* E*cosystem*, Gordon and Breach, 1997, 204 pp.
[16] D. Thomas and G. S. Dieckmann, *Sea Ice: An Introduction to its Physics, Chemistry, Biology and Geology*, Blackwell, 2003, 402 pp.
[17] Y. P. Doronin and D. E. Kheisin, *Morskoi Led (Sea Ice)*, Gidrometeoizdat, Leningrad, 1975, english translation 1977 by Amerind Publishing, New Delhi, 318 pp.
[18] N. Untersteiner, *The Geophysics of Sea Ice*, vol. 146 of *NATO ASI Series, B: Physics*, Plenum Press, New York, 1986, 1196 pp.
[19] P. Wadhams, *Ice in the Ocean*, CRC Press, 2001, 351 pp.
[20] M. Leppäranta, *The Drift of Sea Ice*, Springer Praxis Books Geophysical Sciences, Springer, Berlin, 2005, 266 pp.
[21] F. Ruedorff, *Annalen d. Phys.*, 1861, **114**, 63.
[22] G. Quincke, *Annalen der Physik, Leipzig*, 1905, **18(11)**, 1.
[23] G. Quincke, *Proc. Royal Soc. London A*, 1905, **76**, 431.
[24] S. Maus, *Prediction of the cellular microstructure of sea ice by morphological stability theory*, 11th Int. Conf. on Physics and Chemistry of Ice, Bremerhaven, Germany, Royal Society of Chemistry, pp. 371–382.
[25] T. Tabata and N. Ono, *Low Temperature Science A*, 1962, **20**, 199.
[26] W. F. Weeks and W. L. Hamilton, *The Amer. Mineralogist*, 1962, **47**, 945.
[27] M. Wakatsuchi and T. Saito, *Ann. Glaciol.*, 1985, **6**, 200.
[28] D. M. Cole, J. P. Dempsey, L. H. Shapiro and V. F. Petrenko, in J. P. Dempsey and Y. D. S. Rajapakse, eds., *Ice Mechanics*, vol. 207, Am Soc. Mech. Engin., pp. 161–178.
[29] R. A. Lake and E. L. Lewis, *J. Geophys. Res.*, 1970, **75**, 583.
[30] L. I. Eide and S. Martin, *J. Glaciol.*, 1975, **14**, 137.
[31] T. M. Niedrauer and S. Martin, *J. Geophys. Res.*, 1979, **84**, 1176.
[32] M. Wakatsuchi, *Contrib. Inst. Low Temp. Sci.*, 1983, **A33**, 29.
[33] M. Wakatsuchi, *Low Temp. Sci.*, 1977, **A35**, 249.

[34] J. S. Wettlaufer, M. G. Worster and H. E. Huppert, *J. Fluid Mech.*, 1997, **344**, 291.
[35] K. O. Bennington, *J. Glaciol.*, 1963, **4**, 669.
[36] L. H. Shapiro and W. F. Weeks, in Y. D. S. R. J. P. Dempsey, Z. P. Bazant and S. Shyam, eds., *Ice Mechanics*, vol. 163, Am Soc. Mech. Engin., pp. 177–188.
[37] F. Cottier, H. Eicken and P. Wadhams, *J. Geophys. Res.*, 1999, **104**, 15859.
[38] A. Kovacs, Sea ice: Part I. Bulk salinity versus flow thickness, CRREL Report 96-7, U.S. Army Cold Regions Research and Engineering Laboratory, 1996.
[39] W. F. Weeks, in *Arctic sea ice*, vol. 598, Proc. Conf.on Arctic Sea Ice, Natl. Acad. Sci., pp. 96–98.
[40] J. D. Harrison and W. A. Tiller, *J. Applied Physics*, 1963, **34**, 3349.
[41] P. A. Shumskii, *Osnovy strukturnogo ledovedeniya (Principles of structural glaciology)*, Dover Publications, Inc., 1955, 1964 translated from Russian, 497 pp.
[42] C. A. Knight, *J. Glaciol.*, 1962, **4**, 319.
[43] N. V. Cherepanov and A. V. Kamyshnikova, in G. N. Yakovlev, ed., *Studies in Ice physics and ice engineering (fiziko-tekhnicheskie issledovaniya l'da)*, Israel Program for Sceintific Translations, Gidrometeorologichevskoe Izdatel'stvo (Transalted from Russian), pp. 170–176.
[44] W. F. Weeks and J. S. Wettlaufer, in *The Johannes Weertman Symposium*, The Minerals, Metals and Materials Society, pp. 337–350.
[45] N. K. Sinha, *J. Glac.*, 1978, **21**, 385.
[46] D. K. Perovich and A. J. Gow, *J. Geophys. Res.*, 1996, **101**, 18327.
[47] D. M. Cole and L. H. Shapiro, *J. Geophys. Res.*, 1998, **103**, 21739.
[48] H. Eicken, C. Bock, R. Wittig, H. Miller and H.-O. Poertner, *Cold Reg. Sci. and Technology*, 2000, **31**, 207.
[49] B. Light, G. A. Maykut and T. C. Grenfell, *J. Geophys. Res.*, 2003, **108**, 3051.
[50] D. K. Perovich and A. J. Gow, *J. Geophys. Res.*, 1991, **96**, 16943.
[51] N. K. Sinha, *J. Glac.*, 1977, **18**, 315.
[52] J. Weissenberger, G. Dieckmann, R. Gradinger and M. Spindler, *Limnol. Oceanogr.*, 1992, **37**, 179.
[53] T. Kawamura, *J. Geophys. Res.*, 1988, **93**, 2343.
[54] W. A. Edelstein and E. M. Schulson, *J. Glaciol.*, 1991, **37**, 177.
[55] C. Bock and H. Eicken, *Ann. Glaciol.*, 2005, **40**, 179.
[56] J. Freitag, F. Wilhelms and S. Kipfstuhl, *J. Glaciol.*, 2004, **50**, 243.
[57] F. Flin, J. B. Brzoska, B. Lesaffre, C. Coleou and R. A. Pieritz, *Annals Glaciol.*, 2004, **38**, 39.
[58] M. Schneebeli and S. A. Sokratov, *Hydrol. Processes*, 2004, **18**, 3655.
[59] K. M. Golden, H. E. A. Heaton, J. Miner, D. J. Pringle and J. Zhu, *Geophys. Res. Lett.*, 2007, **34**, L16501.
[60] J. H. Kinney and M. C. Nichols, *Annu. Rev. Mater. Sci.*, 1992, **22**, 121.
[61] M. Stampanoni, G. Borchert, P. Wyss, R. Abela, B. Patterson, S. Hunt, D. Vermeulen and P. Rüegsegger, *Nucl. Instr. Meth. Phys. Res. A*, 2002, **491**, 291.
[62] M. M. Miedaner, T. Huthwelker, F. Enzmann, M. Kersten, M. Stamponi and M. Amman, *X-ray tomographic characterization of impurities in polycrystalline ice*, 11th Int. Conf. on Physics and Chemistry of Ice, Bremerhaven, Germany, Royal Society of Chemistry, pp. 399–408, in press.
[63] M. M. Miedaner, Ph.D. thesis, Institute of Environmental Sciences, Johannes Gutenberg University Mainz, 2007, 113 pp.

[64] M. C. Flemings, *Solidification Processing*, McGraw-Hill, Inc., 1974, 364 pp.
[65] H. E. Huppert, *J. Fluid Mech.*, 1990, **212**, 209.
[66] C. Beckermann, *Int. Materials Reviews*, 2002, **47**, 243.
[67] W. W. Mullins and R. F. Sekerka, *J. Appl. Phys.*, 1964, **35**, 444.
[68] S. Maus, *On Brine Entrapment in Sea Ice: Morphological Stability, Microstructure and Convection*, Logos, Berlin, 2007, 538 pp.
[69] S. Maus, in M. Leppäranta, ed., *Report Series of Geophsyics, University of Helsinki*, p. this volume.
[70] N. V. Cherepanov, *Probl. Arkt. Antarkt.*, 1971, **38**, 137.
[71] A. Kovacs and R. M. Morey, *J. Geophys. Res.*, 1978, **83**, 6037.
[72] W. F. Weeks and A. J. Gow, *J. Geophys. Res.*, 1978, **83**, 5105.
[73] W. F. Weeks and A. J. Gow, *J. Geophys. Res.*, 1980, **85**, 1137.
[74] P. J. Langhorne and W. Robinson, *Cold Reg. Sci. Techn.*, 1986, **12**, 197.
[75] E. Stander and B. Michel, *Cold Regions Sci. Tech.*, 1989, **17**, 153.
[76] M. Nakawo and N. K. Sinha, *Atmos.-Ocean*, 1984, **22**, 193.
[77] N. K. Sinha and C. Zhan, *J. Mater. Sci. Letters*, 1996, **15**, 2118.
[78] E. Stander, in *Int. Conf. on Port and Ocean Engineering*, vol. 1, Narssarssuaq, Greenland, pp. 168–176.
[79] J. D. Harrison, *J. Appl. Phys.*, 1965, **36**, 326.
[80] D. L. Anderson and W. F. Weeks, *Trans. Amer. Geophys. Union*, 1958, **39**, 632.
[81] A. Assur, in *Arctic Sea Ice*, vol. 598, Proc. Conf.on Arctic Sea Ice, Natl. Acad. Sci., pp. 106–138.
[82] V. L. Tsurikov, *Okeanologiia*, 1965, **5**, 463.
[83] C. Petrich, P. J. Langhorne and Z. F. Sun, *Cold Reg. Sci. Techn.*, 2006, **44**, 131.
[84] K. Brattkus, *J. Phys. France*, 1989, **50**, 2999.
[85] L. Rayleigh, *Proc. Royal Soc. London A*, 1879, **29**, 71.
[86] P. Kurowski, S. Cheveigne, G. Faivre and C. Guthmann, *J. Phys. France*, 1989, **50**, 3007.
[87] M. Conti and U. M. B. Marconi, *Phys. Rev. E*, 2000, **63**, 011502.
[88] D. M. Cole, H. Eicken, K. Frey and L. H. Shapiro, *J. Geophys. Res.*, 2004, **109**, C08012.
[89] C. Krembs, T. Mock and R. Gradinger, *Polar Biol.*, 2001, **24**, 356.
[90] C. J. Mundy, D. G. Barber, C. Michel and R. F. Marsden, *Polar Biol.*, 2007, **30**, 1099.
[91] M. Wakatsuchi, *Low Temp. Sci.*, 1974, **A32**, 195.
[92] G. Z. Gershuni and E. Zhukovitskii, *Convective stability of incompressible fluids*, Israel Program for Scientific Translations, Keter Publishing House, in russian 1972 by Izdatel'stvo Nauka, Jerusalem, 1976, 329 pp.
[93] S. Maus, J. Freitag and J. Weissenberger, Backbone and permeability of young sea ice, manuscript in preparation, 2008.
[94] N. Ono, in *Int. Conference on Low Temperature Science*, vol. 1, Ints. of Low Temperature Science, Sapporo, pp. 599–610.
[95] I. Melnikov, *J. Geophys. Res.*, 1995, **C3**, 4673.
[96] J. R. Addison, *J. Glaciol.*, 1977, **18**, 117.
[97] W. S. Reeburgh and M. Springer-Young, *J. Geophys. Res.*, 1983, **88**, 2959.
[98] L. G. Anderson and E. P. Jones, *J. Geophys. Res.*, 1985, **90**, 9194.
[99] M. A. Granskog, K. Virkkunen, D. N. Thomas, H. Kola and T. Martma, *J. Glciol.*, 2004, **50**, 292.

[100] W. Schwarzacher, *J. Geophys. Res.*, 1959, **64**, 2357.
[101] K. O. Bennington, *J. Glaciol.*, 1967, **6**, 845.
[102] T. Saito and N. Ono, *Low Temp. Sci.*, 1977, **A39**, 127.
[103] J. L. Tison and V. Verbeke, *Ann. Glaciol.*, 2001, **33**, 13.
[104] S. Martin, *J. Glaciol.*, 1979, **22**, 473.
[105] J. Freitag, Ph.D. thesis, Universität Bremen, Fachbereich Physik/Elektrotechnik, 1999, auch: Ber. z. Polarforsch., Bd. 325, 1999.
[106] G. F. N. Cox and W. F. Weeks, *J. Glaciol.*, 1986, **32**, 371.
[107] K.-K. Koo, R. Ananth and W. N. Gill, *Phys. Rev. A*, 1991, **44**, 3782.
[108] H. R. Pruppacher and J. D. Klett, *Microphysics of clouds and precipitation*, vol. 18 of *Atmospheric and oceanographic sciences library*, Kluwer Acadamics Publ., 2nd edn., 1997, 954 pp.
[109] B. Light, G. A. Maykut and T. C. Grenfell, *J. Geophys. Res.*, 2004, **109**, C06013.
[110] J. Zhu, A. Jabini, K. M. Golden, H. Eicken and M. Morris, *Ann. Glaciol.*, 2006, **44**, 129.
[111] K. M. Golden, A. Heaton, H. Eicken and V. Lytle, *Mechanics of Materials*, 2006, **38**, 801.
[112] T. Koop, A. Kapilashrami, L. T. Molina and M. J. Molina, *J. Geophys. Res.*, 2000, **105**, 26393.
[113] H. Cho, P. B. Shepson, L. A. Barrie, J. P. Cowin and R. Zaveri, *J. Phys. Chem. B*, 2002, **106**, 11226.
[114] C. A. Knight, *J. Geology*, 1962, **70**, 240.